LATVIAN JOURNAL OF PHYSICS AND TECHNICAL SCIENCES
2015, N 4
DOI: 10.1515/LPTS-2015-0020

DIGITALLY CONTROLLED 4-PHASE BI-DIRECTIONAL INTERLEAVED DC-DC CONVERTER WITH COUPLED INDUCTORS

K. Kroics, U. Sirmelis, L. Grigans

Institute of Physical Energetics
21 Aizkraukles Str., Riga, LV-1006, LATVIA
e-mail: kaselt@inbox.lv

The main advantages of multiphase interleaved DC-DC converters over single-phase converters are reduced current stress and reduced output current ripple. Nevertheless, inductor current ripple cannot be reduced only by an interleaving method. The integrated magnetic structure can be used to solve this problem. In this paper, the application of 2-phase coupled inductor designed in a convenient way by using commercially manufactured coil formers and ferrite cores is analysed to develop a 4-phase interleaved DC-DC converter. The steady state phase and output current ripple in a boost mode of the interleaved bidirectional DC-DC converter with integrated magnetics are analysed. The prototype of the converter has been built. The experimental results of the current ripple are presented in the paper.

Keywords: *DC-DC power converters, integrated magnetics, multiphase switching converters.*

1. INTRODUCTION

Switching power converters have become increasingly important in the industry today. Interfacing the energy sources and storage devices, such as fuel cells, batteries and supercapacitors, requires several DC-DC conversion functions. In many applications such as photovoltaic arrays, fuel cells, wind generators, the high efficiency, small size DC-DC converters are required as an interface between the voltage source and the output loads, which operates at different voltage levels. Bidirectional interleaved DC-DC converters are widely used for management of power flow of the energy storage in automotive application [1], [2], [3], [4], [5], [6]. Merits of the interleaved control methods are reduction of input/output current ripple and volume of the converter, as well as increase in the processed power capacity of the converters. Figure 1 [7] shows the normalised output current ripple according to the number of phases (N) and duty cycle. It shows that by using an interleaved structure current ripple can be significantly reduced. As can be seen from Fig. 1, interleaving of four phases reduces output current ripples in a wide range; therefore, 4-phase boost converter structure is selected. Multiphase interleaved approach employing phase-shifted pulse width modulation (PWM) to control MOSFETs is often used in designs, where paralleling of semiconductor devices is required. The phases are kept independent by using discrete inductors in each phase. Feature of the independent phase approach is the ability to turn-off the individual phases when the output power decreases; this allows maximising the efficiency in each operating point.

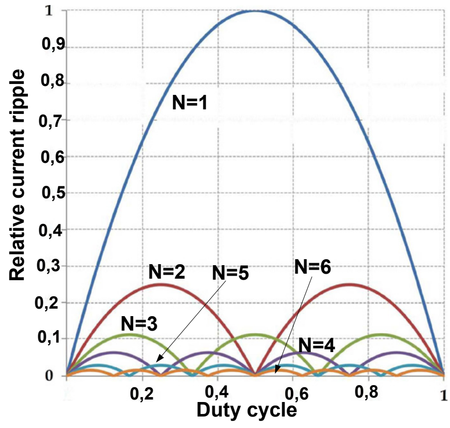

Fig. 1. Normalised output current ripple of boost converter [7].

The interleaving technique allows improving the design of the inductors of the converter. Therefore, demand for compact and lightweight magnetic components is high. In the recent years, energy transfer among phases by means of magnetic coupling has been used in multiphase converters [8]–[16] to reduce size of magnetics.

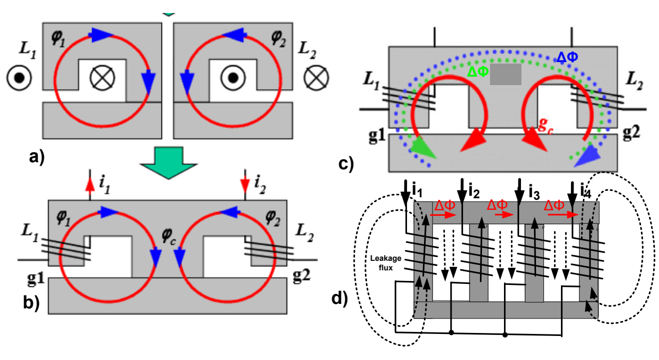

Fig. 2. Magnetic integration principle: a) single inductors; b) parallel coils sharing part of the core; c) increasing the coupling with a gap in the central leg; d) multiphase magnetic integration.

The geometric definition of the integrated cores can be performed looking at the general principle of paralleling of the magnetic circuits (Fig. 2). In Fig. 2a, two separate inductors with a single gapped core are shown. The windings produce a magnetic flux through the magnetic circuit as shown by the arrows. In Fig. 1b, the cores of the inductors of different phases of an interleaved converter are combined, sharing a central leg. As magnetic resistance of the central leg is low, only a small part of magnetic flux goes through the other winding. If the air gap in the central leg is introduced (Fig. 2c), then AC component of flux ($\Delta\Phi$) goes through the second winding and acts like a transformer reducing per-phase current ripple. The central leg has a lower flux level and, therefore, the size of magnetic component can be reduced. If an interleaved converter has many phases (Fig. 2d), then output current ripple is eliminated by interleaving and small inductance is necessary; therefore, a magnetic leg for DC magnetic flux can be removed.

In [3], an approach is proposed based on ferrite material core with high permeability for a coupled inductor with high coupling, which cancels DC flux in the core. Additional inductor is designed by using the dust permalloy material core with high saturation flux density (B_{SAT}) performance. However, it should be taken into account that using the dust material core in an inductor design, costs increase and the power conversion efficiency decreases under low load condition. In the other approach, the inductor and transformer are integrated in one ferrite core [8], [9], [12], [13], [15], [16]. Advantage of this solution is low cost, low loss by high switching frequency. Disadvantage of the ferrite core is low B_{SAT}; to overcome this, the resistance for differential flux must be low to cancel DC flux. By using traditional E-E cores, it is difficult to design and manufacture such an inductor [15] in high coupling coefficient area. There is also a solution to introduce the air gap in the core in order to reduce magnetic flux and design a coupled inductor with coupling less than 1. Most of the proposed coupled inductor structures in the scientific papers cannot be designed in a convenient way by using commercially manufactured coil formers. In this paper, it is offered to design a 2-phase coupled inductor and to develop a 4-phase interleaved DC-DC converter by using this inductor.

2. THE PROPOSED CONVERTER AND COUPLED INDUCTOR

The proposed DC/DC converter will be provided for supercapacitor-based energy storage system. Figure 3 shows the structure of this bidirectional DC-DC converter. Transistors VT_1 to VT_8 are controlled by pulse width modulation. Each parallel pair of switches turns on with shifting of 90 degrees. The switching frequency of the converter will be 50 kHz. To control this DC/DC converter, digital control will be used. The advantage of the digital controller is that it is programmable and offers more functionality to the system compared to the analogue controllers. Novel control algorithms and methods with digital control can be implemented. Such a converter can be used in many other applications; it can be modified as only buck or boost converter because synchronous rectification has better efficiency than diodes. For the assessment of pulsation of current in a 4-phase interleaved DC-DC boost mode of the converter is further analysed.

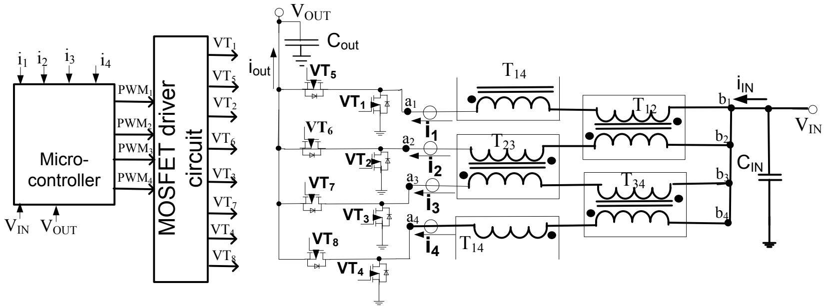

Fig. 3. The schematics of the interleaved DC-DC converter.

The structure of the proposed integrated inductor is shown in Fig. 4. The both windings of the inductors are built on the central leg of E core. Although in literature [8] it is proposed to place windings of the inductor on the wing legs thereby obtaining higher leakage inductance, commercially manufactured coil formers are not available for such a case. In this paper, the proposed inductor can be wound on ETD coil former in a convenient way. Figure 5 shows the practical implementation of the coupled inductor of two phases. The windings of the first phase (2) and windings of the second phase (3) are separated by isolating material (1) and are placed on the coil former (4). The winding machine (5) can be used to build such an inductor.

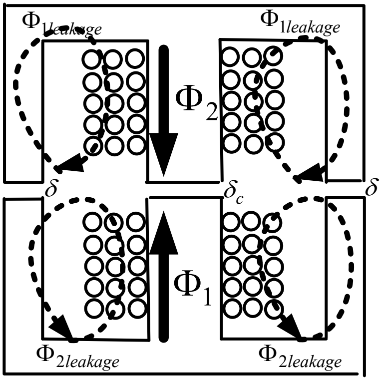

Fig. 4. Core structure of the coupled inductor.

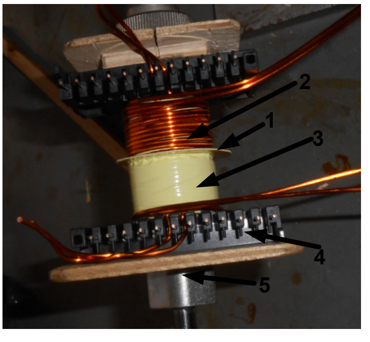

Fig. 5. Practical design of the coupled inductor.

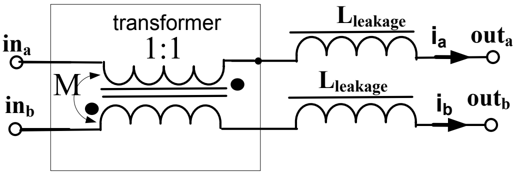

Fig. 6. Equivalent circuit of the inversely coupled inductors.

The equivalent circuit of a two-phase coupled inductor is shown in Fig. 6. Mutual inductance M represents the coupling between the two inductors. The voltages across the two inductors ($v_{inaouta}$, $v_{inboutb}$) are related to the currents through them (i_a, i_b) as follows:

$$v_{in_a\_out_a} = (L_{leakage} + M)\frac{di_a}{dt} - M\frac{di_b}{dt}. \tag{1}$$

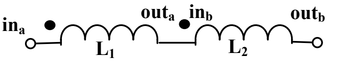

Fig. 7. Measuring of inductance.

It is difficult to calculate a precise value of inductance and coupling coefficient; therefore, it is easier to measure these values and to change air gaps of the inductor in order to achieve the desired values. To measure a coupling coefficient, both windings must be connected in series and total inductance of this connection must be measured (Fig. 7). This inductance can be expressed as follows:

$$L_{total} = L_1 + L_2 + 2M. \tag{2}$$

If the both inductances are equal ($L_1 = L_2 = L$), then mutual inductance can be expressed as follows:

$$M = \frac{L_{total} - 2L}{2}. \tag{3}$$

Coupling coefficient is equal to:

$$k = \frac{M}{L}. \tag{4}$$

3. ASSESSMENT OF OUTPUT CURRENT RIPPLE OF THE CONVERTER

The proposed 4-phase converter shown in Fig. 3 describes such a system of equations:

$$\begin{aligned}
v_{a_1b_1} &= 2L\frac{di_1}{dt} - M\frac{di_2}{dt} - M\frac{di_4}{dt}\\
v_{a_2b_2} &= 2L\frac{di_2}{dt} - M\frac{di_1}{dt} - M\frac{di_3}{dt}\\
v_{a_3b_3} &= 2L\frac{di_3}{dt} - M\frac{di_2}{dt} - M\frac{di_4}{dt}\\
v_{a_4b_4} &= 2L\frac{di_4}{dt} - M\frac{di_3}{dt} - M\frac{di_1}{dt}
\end{aligned}. \tag{5}$$

The sum of all equations in (5) is equal to:

$$(2L-2M)(\frac{di_1}{dt}+\frac{di_2}{dt}+\frac{di_3}{dt}+\frac{di_4}{dt}) = v_{a_1b_1} + v_{a_2b_2} + v_{a_3b_3} + v_{a_4b_4}\,. \tag{6}$$

As can be seen from the schematics in Fig. 3, input current of the converter is equal to the sum of phase currents:

$$\frac{di_1}{dt}+\frac{di_2}{dt}+\frac{di_3}{dt}+\frac{di_4}{dt}=\frac{di_{in}}{dt}\,. \tag{7}$$

According to the pulse length, there are four operation modes on a 4-phase interleaved converter with coupled inductors. The first mode appears when the duty cycle (D) is less than or equal to 1/4 of the switching period (T). The second mode appears when D is between $T/4$ and $T/2$, and the third mode appears when the duty cycle is between $T/2$ and $3T/4$ and the fourth one – when D exceeds $3T/4$.

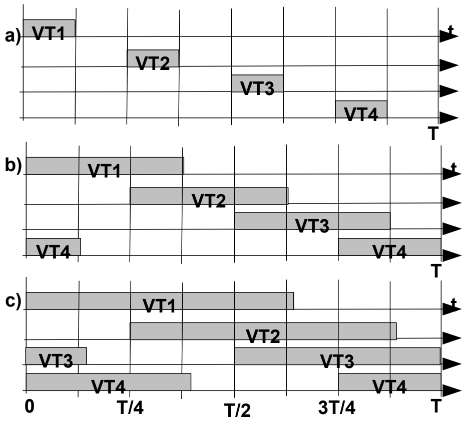

Fig. 8. Operation modes of the interleaved DC-DC converter.

In the first mode, transistor VT1 is on, but transistors VT1, VT2, VT3 are in the “off” state. During the “on” state of the transistors $v_{ab}=V_{IN}$, during the “off” state of the transistor $v_{ab}=V_{IN}-V_{OUT}$. Substituting these expressions depending on the state of transistor (during the first mode negative current ripple can be estimated when all transistors are in the “off” state) in the right part of (6) the following expression can be obtained:

$$v_{a_1b_1} + v_{a_2b_2} + v_{a_3b_3} + v_{a_4b_4} = 4V_{IN} - 4V_{OUT} = 4V_{IN} - 4V_{IN}b\,. \tag{8}$$

The expression for input current (i_{IN}) is obtained as follows by substituting (7) and (8) in (6):

$$\frac{di_{in}}{dt} = \frac{4V_{IN}(1-b)}{2L-2M}. \tag{9}$$

Considering $D = (b\text{-}1)/\mathrm{b}$ and boost ratio $b=V_{OUT}/V_{IN}$ by integrating (9) in the region from DT to $T/4$ (as frequency of input current ripple is 4 times the switching frequency), the expression for input current ripple is obtained:

$$\begin{aligned}\Delta I_{in(D\le 0.25)} &= -\int_{\frac{b-1}{b}T}^{T/4} \frac{4V_{IN}\ 1-b}{2L-2M}dt = \frac{-\left(\frac{-3b+4}{4b}\right)(1-b)4V_{IN}T}{2L-2M} = \\ &= \frac{(4-3b)(b-1)V_{IN}T}{b(2L-2M)}\end{aligned}. \tag{10}$$

In the second mode, current decreases during the period when transistor VT2 is on, but all the other transistors are off. Substituting these expressions depending on the state of transistor in the right part of (6):

$$v_{a_1b_1} + v_{a_2b_2} + v_{a_3b_3} + v_{a_4b_4} = 4V_{IN} - 3V_{OUT} = 4V_{IN} - 3V_{IN}b. \tag{11}$$

The expression for input current (i_{IN}) is obtained as follows by substituting (7) and (8) in (6):

$$\frac{di_{IN}}{dt} = \frac{V_{IN}(4-3b)}{2L-2M}. \tag{12}$$

By integrating (12) in the region from DT to $T/2$, the expression for input current ripple is obtained:

$$\Delta I_{IN(0.25<D<0.5)} = -\int_{\frac{b-1}{b}T}^{T/2} \frac{V_{IN}(4-3b)}{2L-2M}dt = \frac{(3b-4)(2-b)V_{IN}T}{2b(2L-2M)}. \tag{13}$$

In the third mode, current decreases during the period when transistors VT2 and VT3 are on, but transistors VT1 and VT4 are off. By substituting in (6) depending on the state of transistor and integrating in the region from DT to $3T/4$ expression for input current ripple is obtained:

$$\Delta I_{IN(0.5<D\le 0.75)} = -\int_{\frac{b-1}{b}T}^{3T/4} \frac{V_{IN}(4-2b)}{2L-2M}dt = \frac{(b-2)(4-b)V_{IN}T}{2b(2L-2M)}. \tag{14}$$

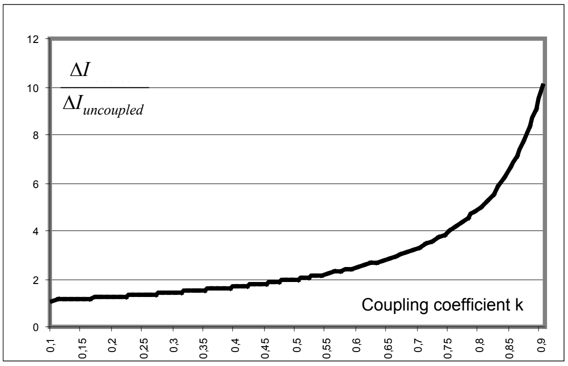

Fig. 9. Input current ripple according to a coupling coefficient.

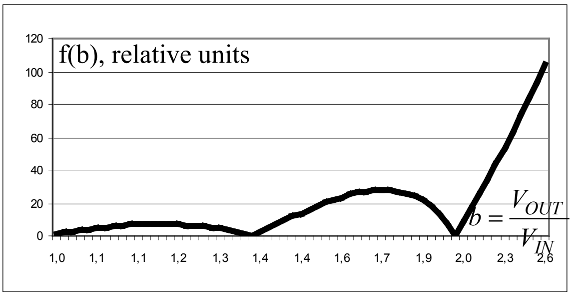

Fig. 10. Input current ripple according to a boost ratio.

From expressions (10), (13), (14) it is possible to draw graphs that describe input current ripple according to a coupling coefficient (Fig. 9) and a boost ratio (Fig. 10). It can be seen that a coupling coefficient higher than 0.9 causes significant input current ripple and, therefore, in this case this coefficient will be considered maximum possible from the current ripple point of view. In the same way, current ripple depends on a boost ratio. In a particular case, a boost ratio will be in the range from 1.1 to 1.7, so the impact in this range is not so considerable.

4. ASSESSMENT OF PER-PHASE CURRENT RIPPLE OF THE CONVERTER

Expression (5) can be overwritten in a matrix form taking into account that $M=kL$:

$$\begin{bmatrix} v_{a_1b_1} \\ v_{a_2b_2} \\ v_{a_3b_3} \\ v_{a_4b_4} \end{bmatrix} = \begin{bmatrix} 2L & -kL & 0 & -kL \\ -kL & 2L & -kL & 0 \\ 0 & -kL & 2L & -kL \\ -kL & 0 & -kL & 2L \end{bmatrix} \cdot \begin{bmatrix} \frac{di_1}{dt} \\ \frac{di_2}{dt} \\ \frac{di_3}{dt} \\ \frac{di_4}{dt} \end{bmatrix}. \tag{15}$$

Eq. 15 can be solved against di_1/dt:

$$\frac{di_1}{dt}=\frac{v_{a_1b_1}(2-k^2)+v_{a_2b_2}k+v_{a_3b_3}k^2+v_{a_4b_4}k}{4L(1-k^2)}=p(k). \tag{16}$$

In the first mode (D<0.25), current increases during the period from 0 to DT. As we have previously established, in such a state of transistors: $V_1=V_{IN}$, $V_2=V_3=V_4=V_{IN}-V_{OUT}$. By inserting these values in (16):

$$\left.\frac{di_1}{dt}\right|_{D\le 0.25}=\frac{V_{IN}(2+2k-k^2b-2kb)}{4L(1-k^2)}=s(k)\ . \tag{17}$$

By integrating (17) in the region from 0 to DT, the expression for phase current ripple is obtained:

$$\left.\Delta I_1\right|_{D\le 0.25}=\int_0^{\frac{b-1}{b}T}s(k)dt=\frac{(2+2k-k^2b-2kb)(b-1)}{4b(1-k^2)}\cdot\frac{TV_{IN}}{L}. \tag{18}$$

Similarly, in the second mode (0.25<D<0.5) current increases during the period from 0 to DT. This period can be divided into three intervals: in the first one $V_1=V_3=V_4=V_{IN}$, $V_2=V_{IN}-V_{OUT}$, in the second one $V_1=V_{IN}$, $V_2=V_3=V_4=V_{IN}-V_{OUT}$, in the third one $V_1=V_2=V_{IN}$, $V_3=V_4=V_{IN}-V_{OUT}$. By inserting these values in (16):

$$\begin{aligned}\left.\Delta I_1\right|_{0.25<D<0.5}&=\int_0^{\frac{b-1}{b}T-\frac{T}{4}}\left.p(k)\right|_{\substack{V_1=V_{IN}\\V_2=V_{IN}\\V_3=V_{IN}\\V_4=V_{IN}-V_{OUT}}}dt+\\&+\int_{\frac{b-1}{b}T-\frac{T}{4}}^{T/4}\left.p(k)\right|_{\substack{V_1=V_{IN}\\V_2=V_{IN}-V_{OUT}\\V_3=V_{IN}-V_{OUT}\\V_4=V_{IN}-V_{OUT}}}dt+\int_{\frac{T}{4}}^{\frac{b-1}{b}T}\left.p(k)\right|_{\substack{V_1=V_{IN}\\V_2=V_{IN}\\V_3=V_{IN}-V_{OUT}\\V_4=V_{IN}-V_{OUT}}}dt\end{aligned}. \tag{19}$$

By solving (19) per-phase current ripple is obtained:

$$\left.\Delta I_1\right|_{0.25<D<0.5}=\frac{(z(k)+bk)(3b-4)-z(k)(b-2)}{8b(1-k^2)}\cdot\frac{TV_{IN}}{L}, \tag{20}$$

From expressions (18) and (20), it is possible to draw graphs that describe phase current ripple according to a boost ratio at different values of the coupling coefficient (Fig. 11). It can be seen that a larger coupling coefficient leads to a decrease in per-phase current ripple only by some values of a boost ratio. This can lead to a false impression that integrating of magnetics does not decrease per-phase current ripple.

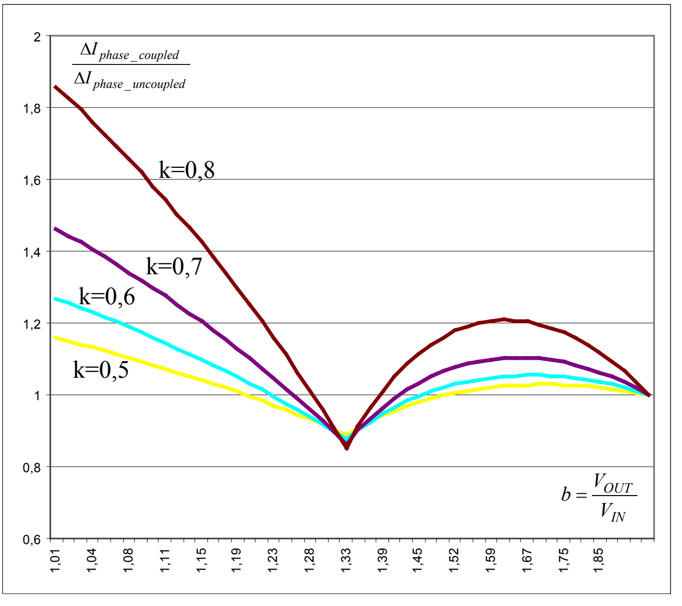

Fig. 11. Per-phase current ripple according to a boost ratio.

To view an impact of integrated magnetics on current ripple reduction, objectively magnetic flux must be taken into account. As can be seen in Fig. 4, magnetic flux that flows through a ferrite core is generated by current difference i_1-i_2 and DC component of current, which creates leakage flux. Assuming the worst case when both currents of coupled inductor are in the opposite phase, then i_1-i_2=$2\Delta I_1$. Taking this into account, equation for flux density B can be written:

$$B = \frac{L(1-k)\cdot I_{IN\_DC}/4}{NA_c} + \frac{2\Delta I_1 L}{NA_c}, \tag{21}$$

where N – a number of turns; A_c – a core cross-sectional area.

As can be seen from (21), flux density through a core can be significantly reduced if a coupling coefficient is equal to 1 (a transformer); in such a case the equation for flux density is:

$$B = \frac{2\Delta I_1 L}{NA_c}. \tag{22}$$

However, as can be seen from Fig. 9, an increase in a coupling coefficient leads to the significant current ripple of output current; therefore, it is necessary to find some compromise between current ripple and flux density.

As for the core materials, ferrite is used and a maximum flux density is set to 0.35 T. If separate inductors are used, then 5 mm air gap is necessary to avoid saturation, at winding count 50 and the inductance equal to 400 μH. If k=1 then M=L=5.6 mH, a very small air gap is necessary, but an additional inductor is required to stay in the continuous conduction mode and to reduce output current ripple, the current regulator must be very advanced as current imbalance leads to saturation of the core of the transformer. In this case, to avoid this problem a coupling coefficient lower than 1 is selected.

5. THE EXPERIMENTAL PROTOTYPE OF THE CONVERTER

The external view of the prototype is shown in Fig.12. In order to control the DC-DC converter, the STM32F407VGT6 microcontroller (MCU) is used. The current of each phase is measured and controlled by PI control algorithm. The PWM signal is shifted in phase by 90 degrees (Fig. 13).

Inductors are wound on ETD59 coil former as shown in Fig. 5. The central air gap and air gaps of outer legs are selected equal to $\delta=\delta_c$=0.5 mm, count of windings is 30, the measured inductance is L=400 μH, coupling coefficient k=0.85. In each phase, there are two inductors in series, it means that inductance is 2 times larger than in case of uncoupled inductor and it is possible to reduce per-phase current ripple by any duty cycle.

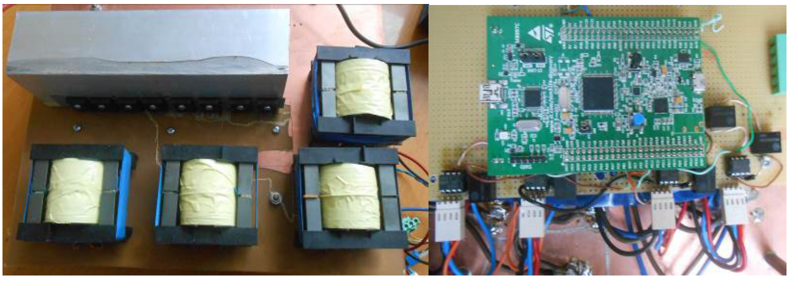

Fig. 12. Prototype of a 4-phase DC-DC converter.

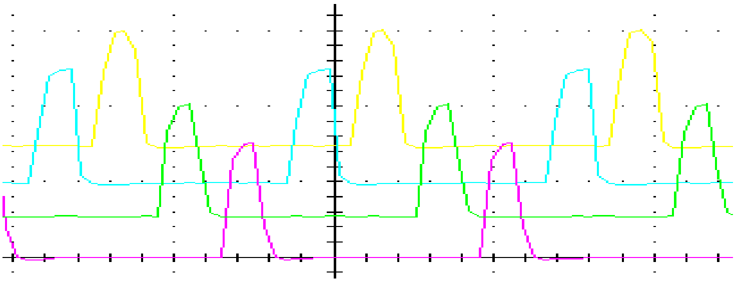

Fig. 13. PWM signals.

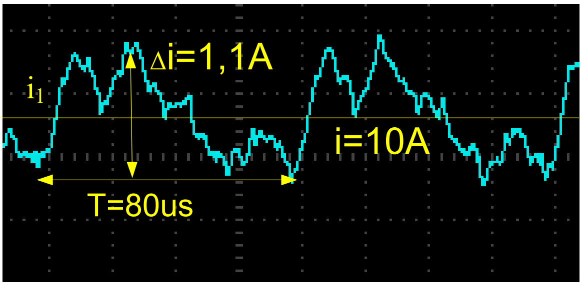

Fig. 14. Phase current *D*=0.1.

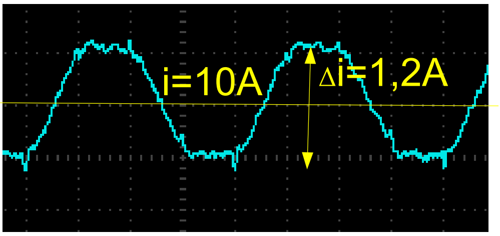

Fig. 15. Phase current *D*=0.25.

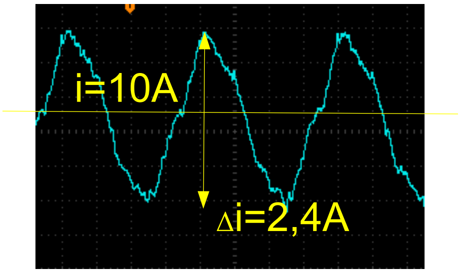

Fig. 16. Phase current *D*=0.37.

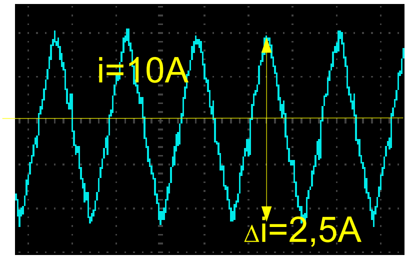

Fig. 17. Phase current *D*=0.5.

Figures 14, 15, 16, 17 show phase current ripple of DC-DC converter at several duty cycles. The switching frequency of the converter in the experiment was equal to only 12.5 kHz since current probe with the bandwidth of 200 kHz was not available. Per-phase current ripple is lower than 25 % of per-phase current and by the proposed switching frequency of 50 kHz per-phase current ripple will be less than 10 %.

6. CONCLUSIONS

In this paper, the design of 4-phase DC-DC converter in respect to per-phase current has been analysed. The application of 2-phase coupled inductor designed in a convenient way by using commercially manufactured coil former ETD has been compared with the uncoupled inductor designed on the same core. The implementation approaches, operational principles and benefits have been analysed in detail based on theoretical and experimental results. The experimental prototype has been developed and experimental results have been shown for verification of the theoretical results. The theoretical expressions for per-phase and input current ripple in the boost mode of the interleaved converter with integrated magnetics have been presented. The experimental results match with the theoretical ones; it can be concluded that the integration of the magnetics allows reducing per-phase current ripple, but input current ripple becomes larger in some working mode. However, interleaving allows maintaining this current ripple at a low level and a small input filter is necessary.

ACKNOWLEDGEMENTS

The research has been supported by the Latvian Council of Science (Project No. 673/2014).

REFERENCES

1. Shrud, A., et al. (2009). Modelling and simulation of automotive interleaved buck converter. In *Universities Power Engineering Conference, UPEC 2009* (pp. 1–6).
2. Jen, C., Li, J., and Sullivan, R. (2003). Automotive application of multi-phase coupled-inductor DC-DC converter. In *IEEE Industry Applications Conference* (pp. 1524–1529). Salt Lake City.
3. Hirakawa, M., Watanabe, Y., Nagano, M., Andoh, K., Nakatomi, S., Hashino, S., and Shimizu, T. (2010). High power DC/DC converter using extreme close-coupled inductors aimed for electric vehicles. In *Power Electronics Conference IPEC 2010* (pp. 2941–2948). Singapore.
4. Jin, K., Yang, M., Ruan, X., and Xu, M. (2010). Three-level bidirectional converter for fuel-cell/battery hybrid power system. *IEEE Transactions on Industrial Electronics 57* (6), 1976–1986.
5. Carpita, M., De Vivo, M., and Gavin, S. (2012). A bidirectional DC/DC interleaved converter for supercapacitor applications. In *Education and Research Conference EDERC 2012* (pp.149–153). Amsterdam.
6. Grbović, P., Delarue, P., Le, P., and Moigne, P. (2010). Bidirectional three-level DC–DC converter for the ultracapacitor applications. *IEEE Transactions on Power Electronics 57* (10), 3415–3430.
7. Taylor, R. PowerLab Notes: When to choose multiphase [online] [16 May 2014]. Available at: http://goo.gl/KVfusd.
8. Womg., P., Peng, X., and Yang, P. (2001). Performance improvements of interleaving VRMs with coupling inductors. *IEEE Transactions on Power Electronics 16* (4), 499–507.

9. Wong, P. (2001). *Performance improvement of multi-channel interleaving voltage regulator modules with integrated coupling inductors*, PhD Dissertation. Dept. Electr.Comput. Eng., Virginia Tech, Blacksburg.
10. Zakis, J., Husev, O., and Strzelecki, R. (2014). Feasibility study of inductor coupling in three-level neutral-point-clamped quasi-Z-source DC/AC converter. In *Electric Power Quality and Supply Reliability Conference, PQ2014* (pp. 273–276). Rakvere.
11. Zhu, G., and Wang, K. (2010). Modelling and design considerations of coupled inductor converters. In *Applied Power Electronics Conference and Exposition APEC 2010* (pp.7–13). Palm Springs.
12. Lee, P., Lee, Y., Cheng, D., and Liu X. (2000). Steady-state analysis of an interleaved boost converter with coupled inductors. *IEEE Transactions on Industrial Electronics 47* (4), 787–795.
13. Santhos, A., et al. (2009). Analysis of coupled inductors for low-ripple fast-response buck converter. *IEICE Transactions on Fundamentals of Electronics, Communications and Computer Sciences 92* (2), 451–455.
14. Zumel, P., et al. (2005). Tight magnetic coupling in multiphase interleaved converters based on simple transformers. In *Applied Power Electronics Conference and Exposition APEC 2005* (pp. 385–391). Austin.
15. Hartnett, K., Hayes J., and Egan, M. (2011). Novel CCTT-core split-winding integrated magnetic for high-power DC-DC converters. In *IEEE Energy Conversion Congress and Expo (ECCE2011)* (pp. 598–605). Phoenix.
16. Laboure, E., Cuniere A., Meynard T. A., Forest, F., and Sarraute, E. (2008). A theoretical approach to Inter-cell transformers, application to interleaved converters. *IEEE Transactions on Power Electronics 23* (1), 464–474.

DIGITĀLI VADĀMS 4 FĀŽU DIVVIRZIENA LĪDZSTRĀVAS PĀRVEIDOTĀJS AR SAISTĪTAJĀM DROSELĒM

K. Kroičs, U. Sirmelis, L. Grigāns

K o p s a v i l k u m s

Šajā rakstā piedāvāta magnētiski saistīta drosele, kas izveidota, izmantojot plaša patēriņa ferrīta serdi un tinuma formētāju. Izmantojot šādas droseles, var tikt izveidots vairākfāžu pārveidotājs ar mazām izejas un iejas strāvas pulsācijām, kā arī samazinātām strāvas pulsācijām droselē. Rakstā sīkāk apskatīts līdzstrāvas pārveidotājs, kas sastāv no četrām fāzēm. Šim gadījumam izvestas teorētiskās formulas strāvas pulsāciju aprēķinam, kā arī rakstā parādīti eksperimentālie rezultāti, kas iegūti, testējot prototipu. Teorētiskie rezultāti sakrīt ar eksperimentālajiem.

13.05.2015.